Geol. Mag. **155** (*8*), *2018, pp. 1667–1683.* © *Cambridge University Press 2017* 1667
doi:10.1017/S0016756817000462

Carbon isotope perturbations and faunal changeovers during the Guadalupian mass extinction in the middle Yangtze Platform, South China

HENGYE WEI*†‡, QUZONG BAIMA†, ZHEN QIU§‡ & CHAOCHENG DAI*

*State Key Laboratory Breeding Base of Nuclear Resources and Environment, East China University of Technology, Nanchang, Jiangxi Province, 330013, China
†School of Earth Science, East China University of Technology, Nanchang, Jiangxi Province, 330013, China
§PetroChina Research Institute of Petroleum Exploration and Development, Beijing 100083, China

(*Received* 17 January 2017; *accepted* 3 May 2017; *first published online* 5 June 2017)

Abstract – The Guadalupian mass extinction took place during the major global environmental changes during Phanerozoic time. Large-scale sea-level fluctuations and a negative shift of $\delta^{13}C$ were associated with this crisis. However, the diagenetic or primary origin of the decreased $\delta^{13}C$ across the Guadalupian–Lopingian (G–L) boundary and the potential causes for this biotic crisis are still being intensely debated. Integrated analyses, including detailed petrographic examination, identification of foraminifer and fusulinid genera, and analysis of carbonate $\delta^{13}C_{carb}$ and bulk $\delta^{13}C_{org}$ across the G–L boundary were therefore carried out at Tianfengping, Hubei Province, South China. Our results show that: (1) some foraminifer and most fusulinid genera disappear in the upper Maokou Formation (upper Guadalupian); (2) the negative shift of $\delta^{13}C_{carb}$ in the uppermost Maokou Formation is of diagenetic origin, but the values of $\delta^{13}C_{carb}$ in the remainder of the Maokou Formation and in the Wuchiaping Formation represent a primary signal of coeval seawater; and (3) the bulk $\delta^{13}C_{org}$ perturbation across the G–L boundary at Tianfengping is mainly controlled by organic matter (OM) source, that is, terrestrial OM contribution. We suggest that the $\delta^{13}C_{carb}$ negative shift in the lower Wuchiaping Formation (Wuchiapingian) compared to that in the lower–middle Maokou Formation (Capitanian) were probably caused by the re-oxidization of ^{12}C-rich OM during regression. Global regression resulted in the negative shift of $\delta^{13}C_{carb}$ at the G–L boundary in South China and led to the loss of shallow-marine benthic habitat. Large-scale global regression is probably one of the main causes for this bio-crisis.

Keywords: Guadalupian–Lopingian, foraminifer, carbon isotope, mass extinction, South China.

1. Introduction

A mass extinction occurred in the Guadalupian epoch (Jin, Zhang & Shang, 1994; Stanley & Yang, 1994; Clapham, Shen & Bottjer, 2009), called the end-Guadalupian mass extinction or pre-Lopingian crisis (Jin, Zhang & Shang, 1994; Stanley & Yang, 1994; Shen & Shi, 1996, 2002; Wang & Sugiyama, 2000) or mid-Capitanian mass extinction (Wignall *et al.* 2009*b*; Bond *et al.* 2010, 2015). This bio-crisis affected marine taxa including fusulinids, small foraminifers, corals, brachiopods, bivalves and ammonoids (Jin, Zhang & Shang, 1994; Wang & Sugiyama, 2000; Weidlich, 2002; Isozaki & Aljinović, 2009; Wei *et al.* 2012; Hada *et al.* 2015; Zhang, Wang & Zheng, 2015). Several geological events have been proposed as the main cause of the mass extinction, including Emeishan volcanism (Zhou *et al.* 2002; Wignall *et al.* 2009*a*; Sun *et al.* 2010), large-scale sea-level fall and loss of shallow-marine habitat (Chen, George & Yang, 2009; Wignall *et al.* 2009*b*; Qiu *et al.* 2014), cooling (Isozaki, Kawahata & Minoshima, 2007; Isozaki, Aljinovic & Kawahata, 2011; Kofukuda, Isozaki & Igo, 2014) and marine anoxia (Isozaki, 1997; Saitoh *et al.* 2013*b*; Zhang *et al.* 2015; Wei *et al.* 2016). However, the causes for this biocrisis are still disputed.

There is a negative excursion of carbon isotope associated with this mass extinction at the Guadalupian–Lopingian (G–L, 259.1 ± 0.5 Ma, Zhong *et al.* 2014) boundary (Wang, Cao & Wang, 2004; Wignall *et al.* 2009*a*; Bond *et al.* 2010). Wignall *et al.* (2009*a*) interpreted the negative excursion of carbon isotope at the G–L boundary as the carbon cycle perturbation resulted from Emeishan volcanism. Further, they suggested that the negative excursion discovered by Wang, Cao & Wang (2004) actually occurred during middle Capitanian time (see also Bond *et al.* 2010). However, Nishikane *et al.* (2014) questioned the volcanic mechanism and middle Capitanian negative excursion of carbon isotope. They argued that the drop in eustatic sea level during Guadalupian time would not be consistent with widespread volcanism since enhanced volcanism is generally associated with a high plate production rate which would result in sea-level rise. The high carbon isotope ratios during middle

‡Authors for correspondence: weihengye@163.com; qiuzhen316@163.com

Capitanian time at Penglaitan global boundary stratotype section and point (GSSP) section (see Chen *et al.* 2011) is also inconsistent with the negative excursion of carbon isotope during middle Capitanian time (Nishikane *et al.* 2014). Instead, they suggested a declined primary production as the cause for the negative excursion at the G–L boundary (Nishikane *et al.* 2014; see also Yan, Zhang & Qiu, 2013). A new interpretation for the negative excursion of carbon isotope at the G–L boundary was suggested by Saitoh *et al.* (2013*a*) who interpreted it as the result of the upwelling of oxygen-depleted water rich in ^{12}C onto the euphotic shelf. Alternatively, Jost *et al.* (2014) questioned the reliability of carbon-isotope negative excursion at the G–L boundary as a primary signal, and interpreted it as local burial conditions or diagenetic origin in some important sections. Accordingly, the interpretation for the carbon isotope negative excursion at the G–L boundary has been highly controversial, and needs more work to reveal the causes of the carbon isotope changes and the kill-mechanism of this extinction. Combining detailed petrographic analysis via thin-section, we have analysed facies, foraminifer fossils record, carbonate-carbon and bulk organic-carbon isotope changes across the G–L boundary at the Tianfengping section in Enshi city (in Hubei Province) in the middle Yangtze Platform, South China. Our results show a different interpretation for the carbon isotope changes during the boundary interval.

2. Geological background

The road-side Tianfengping section (30° 19′ 37″ N, 109° 18′ 52″ E) is located at the Tianfengping village in Enshi city in western Hubei Province, South China. The Tianfengping section crops out over the Maokou Formation, Kuhfeng Formation and Wuchiaping Formation, in ascending order. A detailed description of lithology and interpretation is provided in Section 4. Located in the eastern Palaeo-Tethys ocean in the tropical zone (Scotese & Langford, 1995, p. 3; Muttoni *et al.* 2009), the South China Block was during Capitanian time a large carbonate platform divided by the deep-water Jiangnan Basin in the middle into the Yangtze Platform in the west and the Cathaysian Platform in the east (Fig. 1). The Xiakou-Lichuan Bay (Yin *et al.* 2014) was located in the northern Yangtze Platform (Fig. 1). Our studied section at Tianfengping was located in the centre of this bay. The Kangdian old land was located in the west of the Yangtze Platform.

From middle Capitanian time, the Emeishan large igneous province (LIP) erupted in the southwestern Yangtze Platform (Ali *et al.* 2005; Wignall *et al.* 2009*a*), resulting in a large volcanic and volcaniclastic succession which accumulated across the G–L boundary. The volume of Emeishan LIP was from 0.3×10^6 km^3 (Xu *et al.* 2001) to 0.6×10^6 km^3 (Yin *et al.* 1992, p. 146), only about one-tenth of the Siberian LIP with a volume of 4×10^6 km^3 (Courtillot, 1999). Several rift basins including the Qianzhong basin near Guiyang in Figure 1 (Chen *et al.* 2003) and the Xiakou-Lichuan Bay were suggested to be of rift origin by Zhu (1989), which may be related to the thermal decay of the Emeishan plume.

3. Methods

One hundred samples were collected at Tianfengping with a *c.* 25 cm sample interval, avoiding weathered samples. One hundred thin-sections were created for petrographic examination and identification of fossils.

For inorganic-carbon isotope measurements, we prepared 57 samples of bulk carbonate rock. For each sample, a fresh chip was ground using an agate mortar. Powdered samples were dissolved in phosphoric acid to release CO_2 at Kiel IV of automated carbon reaction device, which was coupled with a Finnigan MAT 253 mass spectrometer for $\delta^{13}C$ and $\delta^{18}O$ measurements. All C-isotope ratios are calibrated to V-PDB using NBS-19. Analytical precision for $\delta^{13}C$ and $\delta^{18}O$ is ±0.04 ‰ and ±0.08 ‰ (1σ), respectively. This experiment was carried out at the Nanjing Institute of Geology and Palaeontology, Chinese Academy of Sciences.

For bulk organic-carbon isotope analyses, 84 samples were powdered smaller than 200 mesh using an agate ball mortar. These powdered samples were digested by 6 N HCl to remove all carbonates. The acid-insoluble residues were cleaned and dried, mixed with CuO and sealed *in vacuo* for further furnace processing. The samples were combusted at 800 °C and the released CO_2 was cryogenically extracted and sealed in vacuum tubes for subsequent $^{13}C/^{12}C$ determination using a Finnigan MAT 253 at the Nanjing Institute of Geology and Palaeontology, Chinese Academy of Sciences. Reproducibility was better than ±0.08 ‰ for organic carbon calibrated to a urea (IVA33802174) standard with $\delta^{13}C_{org}$ value of –40.73 ‰. All data are reported in per mille (‰) relative to V-PDB standard.

4. Results

4.a. Lithostratigraphy

The Tianfengping section consists of the middle Permian Maokou and Kuhfeng formations, and the upper Permian Wuchiaping Formation (Fig. 2). The Wuchiaping Formation can be subdivided into the Wangpo Shale Member in the lower part and the Xiayao Limestone Member in the upper part (Feng, Yang & Jin, 1997; p. 75).

4.a.1. Maokou Formation

The Maokou Formation is composed of massive limestones/dolostones and is subdivided into light-grey limestones in the lower part, grey to dark-grey limestones in the middle part and limy dolostones in the upper part (Figs 2, 3a). The limestones in the lower and middle Maokou Formation show abundant stylolites

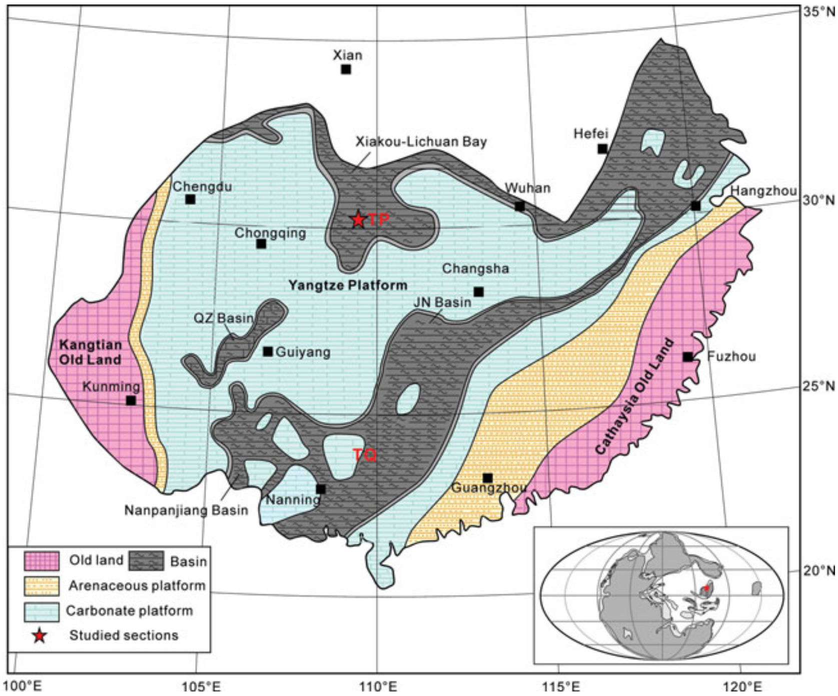

Figure 1. (Colour online) Capitanian palaeogeography of South China (modified from Zhu, 1989; Wang & Jin, 2000; Chen *et al*. 2003; Du *et al*. 2015) and the locations of studied sections. TP – Tianfengping section; QZ Basin – Qianzhong intrashelf basin; JN Basin – Jiangnan basin; TP – Tianfengping section; TQ – Tieqiao section.

and bioturbation (Fig. 2), and contain abundant bioclasts such as brachiopods, crinoids, echinoids, foraminifers, sponge spicules and green calcareous algae (Figs 2, 3b). Non-skeletal grains such as peloids, oncoids and cortoids also occur in the lower and middle Maokou Formation. The limy dolostones in the uppermost Maokou Formation contain dolomite crystals with cloudy centres and clear rims (Fig. 3c), suggesting replacement of limestones. There are also abundant bitumen (Fig. 3d) and small karst caves (Fig. 3e, f) in the uppermost Maokou Formation, suggesting a phase of karstification during sub-aerial exposure. The boundary between the Maokou and Kuhfeng formations is a regional unconformity (Fig. 3a).

4.a.2. Kuhfeng Formation

The 3.8 m-thick Kuhfeng Formation is composed of thin-bed (3–8 cm thick) black cherts interbedded with *c.* 1 cm carbonaceous black shales (Fig. 3a). Authigenic carbonate concretions are common and the largest (*c.* 1 m) occurs in the middle Kuhfeng Formation (Fig. 3g). Microscopically, phylloid algae (Fig. 3h), siliceous sponge spicules (Fig. 3i) and abundant radiolarians (Fig. 3j) occur in the lower, middle and upper parts of Kuhfeng Formation, respectively. Some small ammonoids (Fig. 3k) and brachiopods (Fig. 3l) also occur in the middle Kuhfeng Formation.

4.a.3. Wuchiaping Formation

The Wuchiaping Formation includes the Wangpo Shale Member in the lower part and Xiayao Limestone Member in the upper part. The Wangpo Shale Member consists of lithic arenite and claystones in the lower part and black shale intercalated with thin-bed limestone in the upper part (Fig. 2). Coal is very common in the lower Wangpo Shale Member (Fig. 4a). The lithic arenite contains abundant feldspar and pyrite minerals (Fig. 4b–d) and lithic grains including tuff (Fig. 4e, f), basalt (Fig. 4g), spherulitic rhyolite (Fig. 4h) and chert (Fig. 4i). The tuff grains are very common. Muscovite (Fig. 4j), authigenic gypsum (Fig. 4k) and albite (Fig. 4l) also occur in this sandstone. The claystones overlying the lithic arenite are rich in pyrites (Fig. 4m), and the overlying floatstone contains abundant phylloid green algae (Fig. 4n). The thin-bedded lime mudstones occurred as intercalated bed in the black shale in the upper Wangpo Shale Member, containing abundant small round peloids (Fig. 4o).

The Xiayao Limestone Member in the upper Wuchiaping Formation consists of thin- to thick-bedded argillaceous lime mudstones, wackestones and packstones (Fig. 5a, b). The argillaceous lime mudstones and wackestones display laminations (Fig. 5c) and contain large brachiopods (Fig. 5d–f), partially replaced by authigenic albite (Fig. 5e). The packstones to grainstones in the upper Xiayao Limestone Member contain abundant green algae and sponge spicules, gastropods, brachiopods, foraminifers (Fig. 5g–i) and ubiquitous disseminated glacuconites (Fig. 5h).

4.b. Foraminifer biostratigraphy

Fossil range data show that the Maokou Formation contains a high diversity of nonfusulina foraminifers

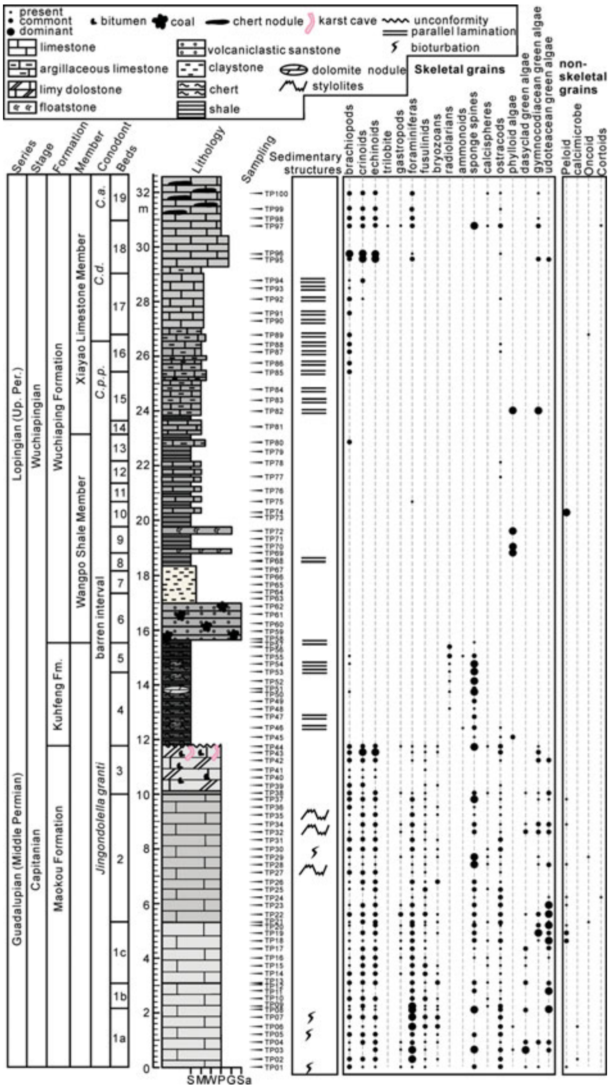

Figure 2. (Colour online) Graphic sedimentary log across the Guadalupian–Lopingian boundary at the Tianfengping section, South China. S – shale; M – lime mudstone; W – wackestone; P – packstone; G – grainstone; Sa – sandstone. The conodont data is from Xia *et al.* (2006). *C. p.p. – Clarkina postbitteri postbitteri*; *C.d. – Clarkina dukouensis*; *C.a. – Clarkina asymmetrica*.

and fusulinids, but that the Wuchiaping Formation only contains a few small foraminifers at Tianfengping (Fig. 6). For the small foraminifers, the long-ranging genera persisting into the Wuchiapingian strata include *Pachyphloia*, *Nodosaria*, *Langella*, *Geinitzina*, *Psedoglandulina*, *Neotuberitina*, *Hemigordius* and *Agathammina* at Tianfengping (Fig. 6), in which *Pachyphloia*, *Nodosaria*, *Geinitzina*, *Hemigordius* and *Agathammina* had been also reported in Wuchiapingian deposits in Guangyuan in South China (Lai *et al.* 2008), at Tieqiao in South China (Wignall *et al.* 2009*b*; Zhang *et al.* 2015) and in Takachiho in Japan (Kobayashi, 2012). The *Globivalvulina*, *Deckerella*, *Palaeotextularia*, *Cribrogenerina*, *Climacammina*, *Tetrataxis*, *Frondicularia*, *Glomospira*, *Cribrogenerina*, *Neodiscus*, *Archaediscus*, *Multidiscus*, *Ammodiscus*, *Plectogyra* and *Robuloides* disappeared in the Wuchiaping Formation at Tianfengping (Fig. 6). However, some of these disappeared genera had been reported in the Wuchiapingian strata elsewhere, such as *Palaeotextularia* in Guangyuan in South China (Lai *et al.* 2008), *Climacammina* in Guangyuan (Lai *et al.* 2008), Laibin (Wignall *et al.* 2009*a*; Zhang *et al.* 2015) in South China and Takachiho in Japan (Kobayashi, 2012), *Frondicularia* in Guangyuan (Lai *et al.* 2008), Laibin Wignall *et al.* (2009*b*) and Takachiho in Japan (Kobayashi, 2012), *Glomospira* in Takachiho in Japan (Kobayashi, 2012), *Neodiscus* in Takachiho in Japan (Kobayashi, 2012), and *Multidiscus* in Laibin in South China (Zhang *et al.* 2015) and Takachiho in Japan (Kobayashi, 2012). Most of the foraminiferal genera therefore persist into the Wuchiapingian stratigraphy and only nine of them disappear from the upper Maokou Formation.

For the fusulinids range data, all of these fusulinid genera identified in the Maokou Formation disappeared in the Kuhfeng and the Wuchiaping formations (Wuchiapingian) at Tianfengping (Fig. 6). They were *Schwagerina*, *Schubertella*, *Reichellina*, *Skinnerella*, *Ozawainella*, *Chenella*, *Chusenella*, *Staffella* and *Nankinella*. However, *Reichellina*, *Codonofusiella*, *Staffella* and *Nankinella* had been reported in Wuchiapingian deposits elsewhere such as Guangyuan (Lai *et al.* 2008), Laibin Wignall *et al.* (2009*b*) in South China (Jin *et al.* 2006) and in Takachiho in Japan (Kobayashi, 2012). Most of the fusulinid genera therefore disappear at 9.5 m in the upper Maokou Formation in the upper Capitanian (e.g. *J. granti* zone; Xia *et al.* 2006) at Tianfengping (Fig. 6).

4.c. Carbon isotope chemostratigraphy

At Tianfengping, carbonate-carbon isotopic ratios $\delta^{13}C_{carb}$ range from –0.7 ‰ to 3.9 ‰ with an average value of 2.3 ‰ (Table 1). The $\delta^{13}C_{carb}$ profile stabilizes at *c.* 3.8 ‰ in the lower and middle Maokou Formation below 9.0 m and shifts to 0.7 ‰ in the upper Maokou Formation (Fig. 7). The $\delta^{13}C_{carb}$ values in the Wuchiaping Formation are relatively low, ranging from 0.2 ‰ to 1.6 ‰ with an average value of 0.8 ‰ (Fig. 7). The $\delta^{13}C_{carb}$ profile in the Wuchiaping Formation shows a gradual positive change from *c.* 0.5 ‰ to 1.60 ‰ (Fig. 7). Carbonate $\delta^{18}O_{carb}$ values range from –7.0 ‰ to –3.5 ‰, with an average value of –5.6 ‰ (Table 1).

Organic-carbon isotopic ratios ($\delta^{13}C_{org}$) range from –28.7 ‰ to –21.5 ‰, with an average value of –26.0 ‰. The $\delta^{13}C_{org}$ profile stabilizes at *c.* –28.4 ‰ in the lower and middle Maokou Formation (below 9.0 m) and shows a positive change from –28.4 ‰ to *c.* –26.5 ‰ in the upper Maokou Formation (Fig. 7). The $\delta^{13}C_{org}$ profile stabilizes at *c.* –26.5 ‰ in the lower Kuhfeng Formation and changes to *c.* –27.1 ‰ in the upper Kuhfeng Formation. At the Kuhfeng–Wuchiaping formation boundary, $\delta^{13}C_{org}$ profile shows an abrupt shift from –26.5 ‰ in the Kuhfeng Formation to –21.5 ‰ in the lower Wangpo Shale Member. The $\delta^{13}C_{org}$ profile then stabilizes at *c.* –23.9 ‰ in the upper Wangpo Shale Member and lower Xiayao

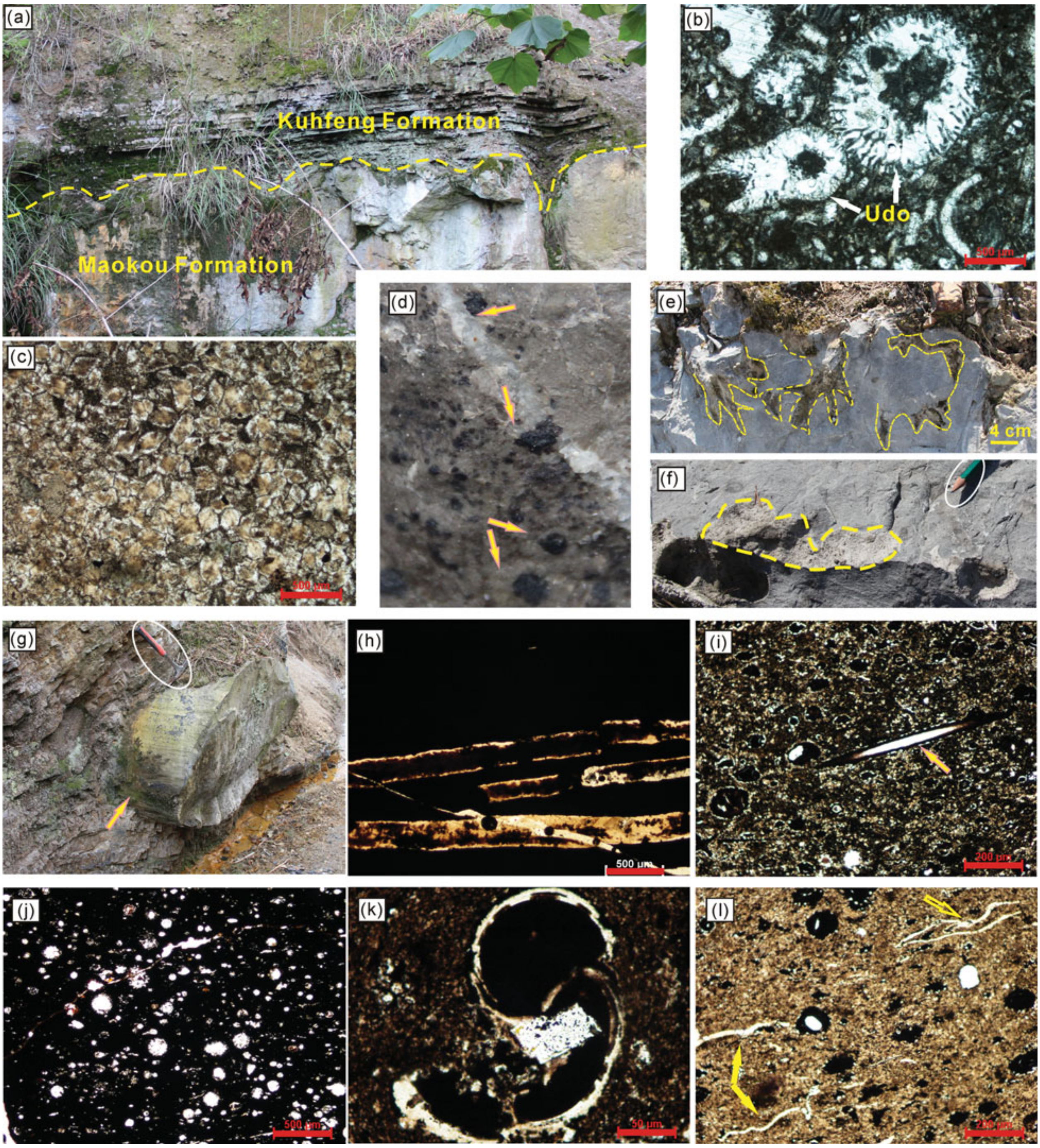

Figure 3. (Colour online) Field photos and thin-section micrographs of the Maokou and Kuhfeng formations at Tianfengping, South China. (a) The Maokou–Kuhfeng boundary; and (b) Udoteacean packstone. Sample TP18. Plane polarized light (PPL). Bar scale 500 μm. (c) Dolomites with cloudy centres and clear rims. Sample TP42. PPL. Bar scale 500 μm. (d) Bitumens (arrows) at the top of the Maokou Formation. Size of bitumen is about 1 cm. (e) Small karst caves (dash lines) at the top of the Maokou Formation. (f) The internal surface of karst cave (dash line) the top of the Maokou Formation. Pencil for scale. (g) Dolomite nodule in the black chert. Hammer for scale. (h) Phylloids in the black chert in the lowermost Kuhfeng Formation. Sample TP45. PPL. (i) Siliceous sponge spicule (arrow) in the black chert. Sample TP50. PPL. (j) Radiolarian chert. Sample TP55. PPL. (h–j) Bar scale 500 μm. (k) Ammonoid in the lower Kuhfeng Formation. Sample TP46. PPL. Bar scale 50 μm. (l) Small and thin-shell brachiopod fragments (solid arrows) and intact one (hollow arrow). Sample TP50. PPL. Bar scale 200 μm.

Limestone Member, and then gradually shifts to –25.8 ‰ in the upper Xiayao Limestone Member (Fig. 7).

In summary, $\delta^{13}C_{carb}$ values in the Wuchiaping Formation are substantially lower than in the Maokou Formation (*c.* 3 ‰ in magnitude). The $\delta^{13}C_{carb}$ values in the upper Maokou Formation are isotopically lighter than in the lower and middle Maokou Formation. The $\delta^{13}C_{org}$ values in the upper Maokou Formation and Kuhfeng Formation are higher than in the lower and middle Maokou Formation, while $\delta^{13}C_{org}$ values in the Wuchiaping Formation are much higher than in the Kuhfeng and Maokou formations. Even in the Wuchiaping Formation, the $\delta^{13}C_{org}$ profile displays

https://doi.org/10.1017/S0016756817000462 Published online by Cambridge University Press

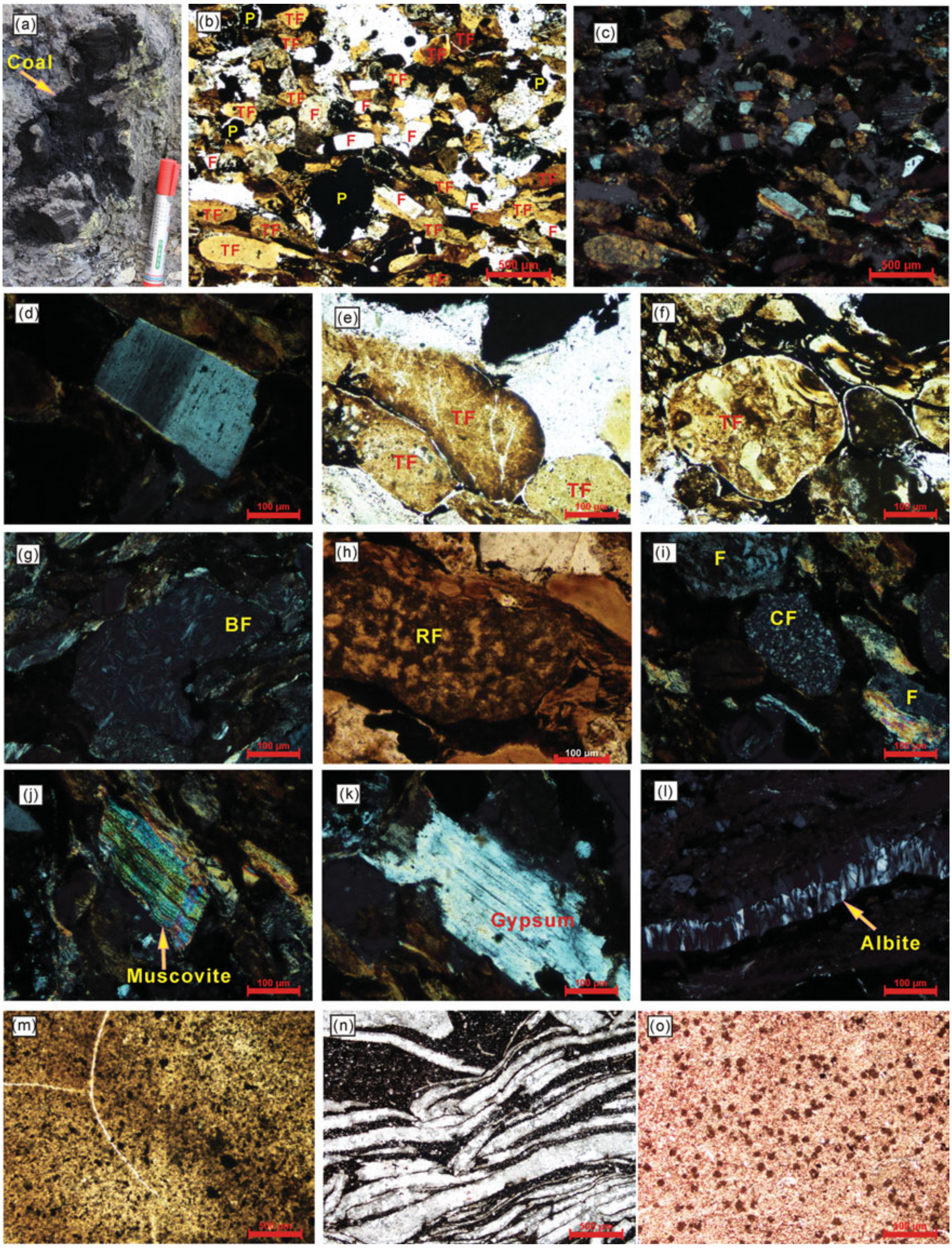

Figure 4. (Colour online) Field photos and thin-section micrographs of the Wangpo Shale Member in the Wuchiaping Formation at Tianfengping. (a) Black coal (arrow). Marker for scale. (b) Feldspar (F), tuff fragment (TF) and pyrite (P) in sandstone. Sample TP59. PPL. Bar scale 500 μm. (c) Cross-polarized light (CPL) of (b). (d) Palgioclase in the sandstones. Bar sample TP 59. CPL. (e) Tuff fragments (TF) showing oxidized rim. Sample TP59. PPL. (f) Tuff fragment (TF) showing glassy fragment (arrow). Sample TP59. PPL. (g) Basaltic fragment (BF) showing angular shape. Sample TP60. CPL. (h) Spherulitic rhyolite fragment (RF). Sample TP59. PPL. (i) Chert fragment (CF) and feldspar (F) grains. Sample TP60. CPL. (j) Muscovite (arrow) grain. Sample TP60. CPL. (k) Authigenic gypsum. Sample TP59. CPL. (l) Authigenic albite in the sandstone. Sample TP62. CPL. (d–l) Bar scale 100 μm. (m) Claystones containing abundant black pyrite. Sample TP67. PPL. (n) Phylloid fragments (light bands) and calcisphere (light spots). Sample TP69. PPL. (o) Peloid wackestone. Sample TP74. PPL. (m–o) Bar scale 500 μm.

https://doi.org/10.1017/S0016756817000462 Published online by Cambridge University Press

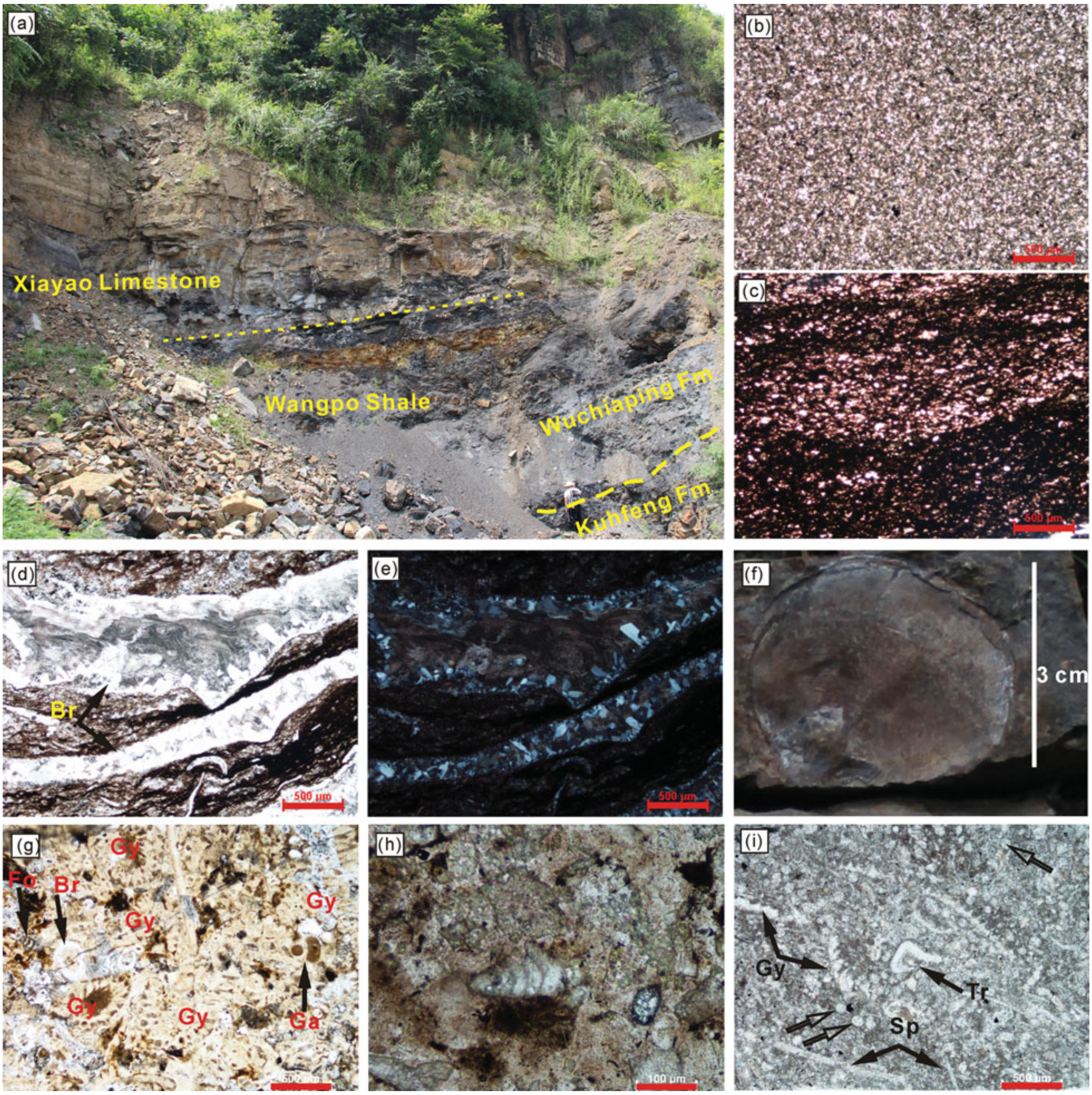

Figure 5. (Colour online) Field photos and thin-section micrographs of the Xiayao Limestone Member in the Wuchiaping Formation at Tianfengping. (a) Outcrop of the Wuchiaping Formation; (b) Lime mudstone, Sample TP 84. PPL. (c) Laminations in the argillaceous lime mudstone. Sample TP83. PPL. (d) Large brachiopods (Br) in the argillaceous lime mudstone. Sample TP86. PPL. (b–d) Bar scale 500 μm. (e) CPL image of (d). Authigenic albites occur in the rim of brachiopod fragments. (f) Brachiopod fossil in Sample TP93 in Bed 17. (g) Gymnocodiacean algae (Gy) grainstone containing small foraminifera (Fo), brachiopod spicule (Br) and gastropod (Ga). Sample TP95. PPL. Bar scale 500 μm. (h) Disseminated glauconites (yellow-green color). Sample TP95. PPL. Bar scale 100 μm. (i) Packstone containing abundant sponge spicules (Sp and hollow arrows), trilobite (Tr) and Gymnocodiacean green algae (Gy). Sample TP97. PPL. Bar scale 500 μm.

three steps from heavier to lighter values in the lower Wangpo Shale Member, upper Wangpo Shale Member to lower Xiayao Limestone Member and upper Xiayao Limestone Member, respectively.

5. Discussion

5.a. Changes in the sedimentary environment

The unconformity at the Maokou–Kuhfeng formation boundary at Tianfengping also occurred in other sections, for example Jianshi and Badong, suggesting a regional regression and sub-aerial exposure in South China (e.g. Chen *et al.* 2000; Niu *et al.* 2000). The occurrence of phylloids and small brachiopods in the black chert of the Kuhfeng Formation suggests that it was not a typical deep-marine environment. The spherical radiolarians which prefer inhabiting relatively shallower-water environments (Kozur, 1993) are abundant in the Kuhfeng Formation at Maocaojie near our studied section (Shi *et al.* 2016). Furthermore, high organic carbon (6 %, Yao *et al.* 2002; 1.5–18 %, Shi *et al.* 2016) in the Capitanian

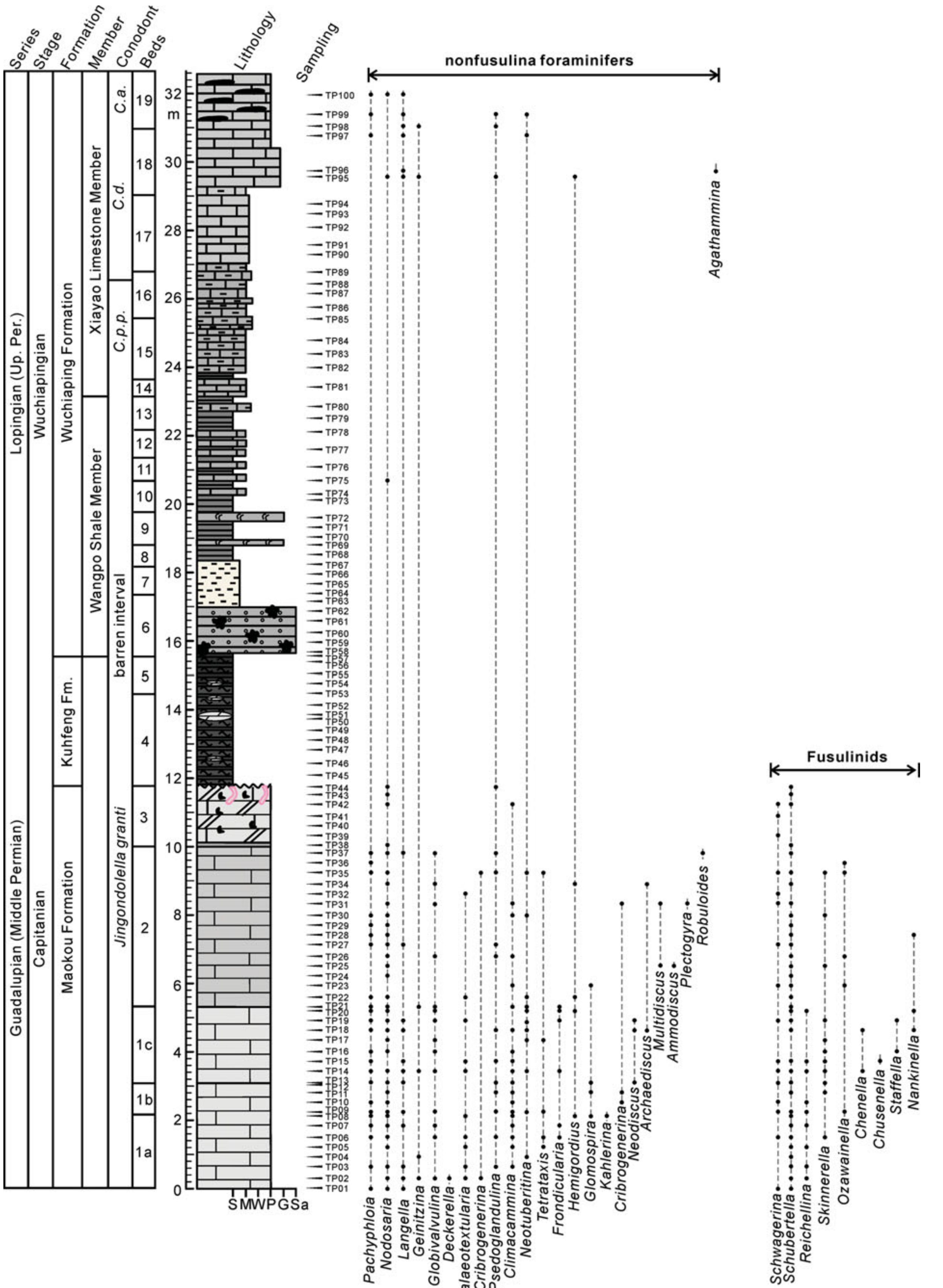

Figure 6. (Colour online) Foraminifera occurrences across the G–L boundary at Tianfengping, South China. For lithologic keys and conodont zones see Figure 2.

https://doi.org/10.1017/S0016756817000462 Published online by Cambridge University Press

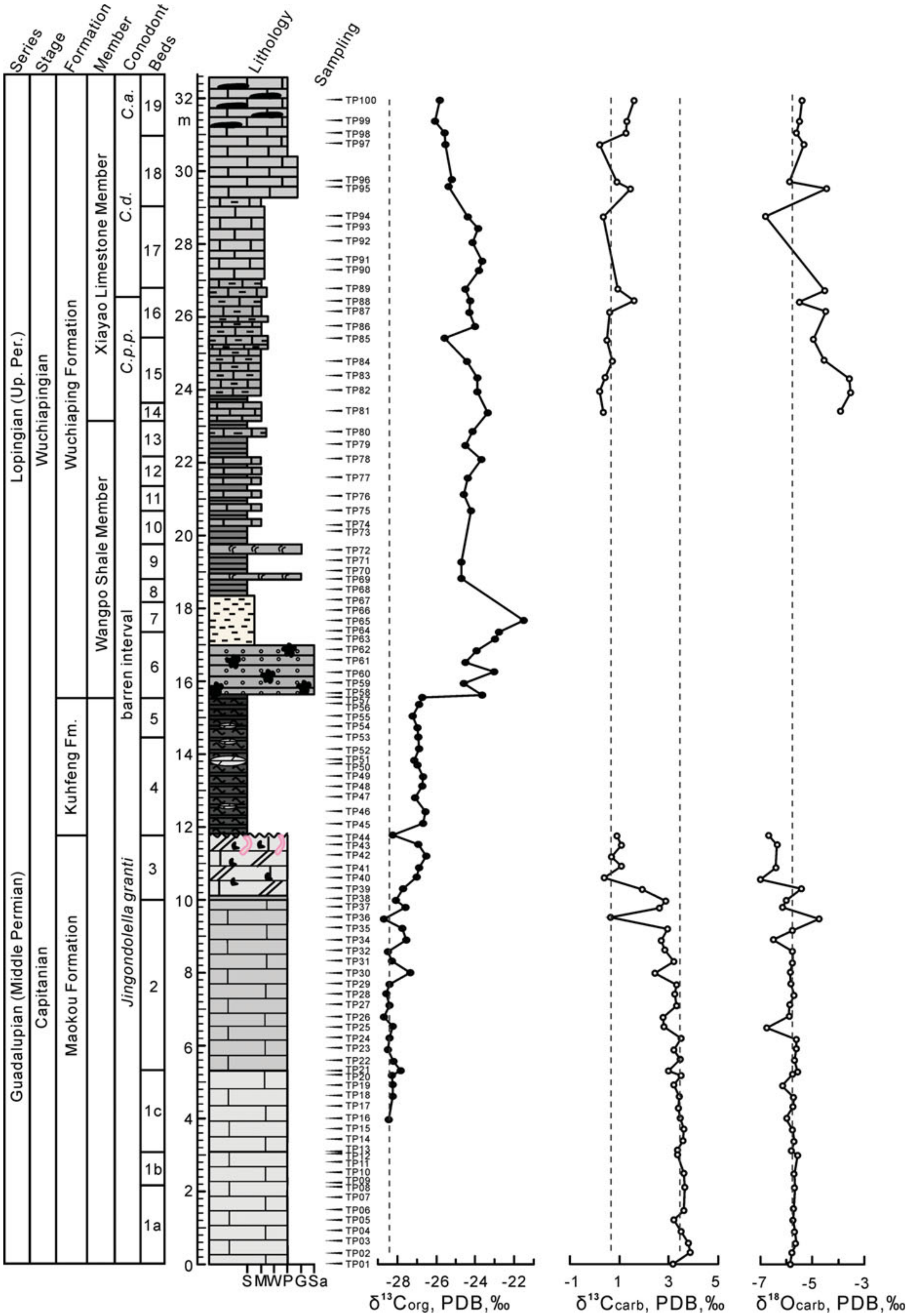

Figure 7. (Colour online) Carbonate-carbon isotope ($\delta^{13}C_{carb}$) and oxygen isotope ($\delta^{18}O_{carb}$), and organic-carbon isotope ($\delta^{13}C_{org}$) profiles across the G–L boundary at Tianfengping, South China. For lithologic keys see Figure 2.

https://doi.org/10.1017/S0016756817000462 Published online by Cambridge University Press

Table 1. Stable carbonate-carbon, bulk organic-carbon, oxygen isotopes and the isotopic difference between carbonate-carbon and organic-carbon isotope data at Tianfengping, South China.

Sample	Thickness (m)	$\delta^{13}C_{org}$ (‰)	$\delta^{13}C_{carb}$ (‰)	$\delta^{18}O_{carb}$ (‰)
Xiayao Limestone Member (Wuchiaping Formation)				
TP100	31.95	−25.8	1.6	−5.4
TP99	31.4	−26.1	1.3	−5.5
TP98	31.05	−25.6	1.3	−5.6
TP97	30.75	−25.5	0.2	−5.3
TP96	29.75	−25.2	0.9	−5.9
TP95	29.55	−25.4	1.5	−4.5
TP94	28.75	−24.4	0.4	−6.8
TP93	28.45	−23.9		
TP92	28.05	−24.1		
TP91	27.55	−23.7		
TP90	27.3	−23.8		
TP89	26.75	−24.5	0.9	−4.5
TP88	26.45	−24.2	1.6	−5.6
TP87	26.15	−24.3	0.6	−4.5
TP86	25.75	−24.0		
TP85	25.4	−25.6	0.5	−5.0
TP84	24.8	−24.4	0.7	−4.5
TP83	24.35	−23.9	0.4	−3.6
TP82	23.95	−23.9	0.2	−3.5
TP81	23.4	−23.4	0.3	−3.9
Wangpo Shale Member (Wuchiaping Formation)				
TP80	22.85	−24.1		
TP79	22.5	−24.5		
TP78	22.1	−23.7		
TP77	21.6	−24.4		
TP76	21.1	−24.6		
TP75	20.7	−24.2		
TP74	20.3			
TP73	20.1			
TP72	19.6			
TP71	19.3	−24.7		
TP70	19			
TP69	18.8	−24.7		
TP68	18.5			
TP67	18.2			
TP66	17.95			
TP65	17.65	−21.5		
TP64	17.35	−22.8		
TP63	17.15	−23.0		
TP62	16.85	−23.9		
TP61	16.55	−24.5		
TP60	16.25	−23.1		
TP59	15.95	−24.6		
TP58	15.65	−23.7		
Kuhfeng Formation				
TP57	15.55	−26.7		
TP56	15.35	−26.9		
TP55	15.05	−27.2		
TP54	14.75	−27.0		
TP53	14.45	−26.9		
TP52	14.15	−26.9		
TP51	13.85	−27.1		
TP50	13.7	−27.0		
TP49	13.4	−26.7		
TP48	13.1	−26.7		
TP47	12.8	−27.1		
TP46	12.4	−26.5		
TP45	12.1	−26.7		
Maokou Formation				
TP44	11.75	−28.3	0.9	−6.7
TP43	11.5	−26.9	1.1	−6.4
TP42	11.2	−26.5	0.7	−7.3
TP41	10.9	−26.9	1.1	−6.4
TP40	10.6	−27.0	0.4	−7.0
TP39	10.3	−27.7	1.9	−5.4
TP38	10	−28.1	2.9	−6.0
TP37	9.8	−27.6	2.6	−6.1
TP36	9.5	−28.7	0.6	−4.7
TP35	9.2	−27.8	2.9	−5.8
TP34	8.9	−27.5	2.7	−6.5

Table 1. Continued.

Sample	Thickness (m)	$\delta^{13}C_{org}$ (‰)	$\delta^{13}C_{carb}$ (‰)	$\delta^{18}O_{carb}$ (‰)
TP32	8.6	−28.5	2.8	−5.8
TP31	8.3	−28.3	3.2	−5.8
TP30	8	−27.3	2.4	−5.8
TP29	7.7	−28.4	3.3	−5.8
TP28	7.4	−28.5	3.3	−5.7
TP27	7.1	−28.4	3.3	−5.9
TP26	6.8	−28.7	2.8	−5.9
TP25	6.5	−28.2	2.8	−6.8
TP24	6.2	−28.4	3.5	−5.6
TP23	5.9	−28.5	3.2	−5.6
TP22	5.6	−28.2	3.4	−5.7
TP21	5.3	−27.8	3.0	−5.6
TP20	5.2	−28.3	3.5	−5.8
TP19	4.9	−28.2	3.2	−6.2
TP18	4.6	−28.2	3.4	−5.7
TP17	4.3		3.4	−5.7
TP16	4	−28.4	3.5	−6.0
TP15	3.7		3.6	−5.8
TP14	3.4		3.6	−5.7
TP13	3.1		3.4	−5.8
TP12	3		3.4	−5.6
TP11	2.8			
TP10	2.5		3.6	−5.7
TP09	2.2			
TP08	2.1		3.7	−5.7
TP07	1.8			
TP06	1.5		3.6	−5.7
TP05	1.2		3.2	−5.7
TP04	0.9		3.5	−5.7
TP03	0.6		3.8	−5.6
TP02	0.3		3.9	−5.8
TP01	0		3.2	−5.9

Kuhfeng Formation at Tianfengping probably suggests a restricted environment with weak water circulation (e.g. Zhang *et al.* 2015; Wei *et al.* 2016; Saitoh *et al.* 2017). The petrography, which is characterized by abundant peloids, sandstones and claystones intercalated with coal beds in the Wangpo Shale Member (Wuchiapingian) (Fig. 4), suggests a coastal swamp environment; the argillaceous limestone and low biodiversity dominated by brachiopods in the low Xiayao Limestone Member (Fig. 5b–f) suggest a restricted environment, however. Abundant authigenic gypsums and albites in the Wangpo Shale Member and lower Xiayao Limestone Member suggest high concentrations of SO_4^{2-} and/or Na^+ in the diagenetic fluids since the gypsums grew in intergranular pore (Fig. 4k) and the albites were formed by the replacement of skeletons such as brachiopods (Fig. 5e). In the upper Xiayao Limestone Member, the packstones/grainstones contain abundant bioclasts with high biodiverisity (Fig. 5g–i) and glauconites, suggesting an open shallow-marine environment. In summary, the lower part of the Wuchiaping Formation (upper Permian) was deposited in a coastal swamp environment. The middle Permian Maokou Formation and the upper part of Wuchiaping Formation (upper Permian) were deposited in shallow-marine environments. The middle Permian Kuhfeng Formation, which is sandwiched between the Maokou and Wuchiaping formations, may have been deposited in a mid-depth

https://doi.org/10.1017/S0016756817000462 Published online by Cambridge University Press

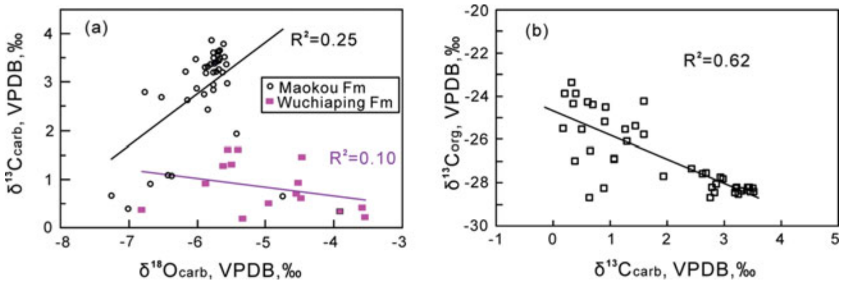

Figure 8. (Colour online) (a) Cross-plot between carbonate-carbon isotope and oxygen isotope at Tianfengping; (b) Cross-plot between carbonate-carbon isotope and organic-carbon isotope.

environment rather than a deep basin. The Kuhfeng Formation elsewhere in South China was also deposited in the water depth not deeper than several hundred metres (Kametaka *et al.* 2005).

5.b. Primary or diagenetic origin of carbon isotope records

5.b.1. $\delta^{13}C_{carb}$ changes

Carbon isotopic ratios can be altered by the post-depositional processes such as meteoric burial and organic diagenesis (e.g. Rosales, Quesada & Robles, 2001). It is critical to assess the diagenetic effect on carbon isotopic composition in order to reconstruct the environmental changes. The oxygen isotope ratios of whole-rock carbonates are generally altered during diagenesis (e.g. Weissert, Joachimski & Sarnthein, 2008). Positive correlations between $\delta^{18}O$ and $\delta^{13}C$ in marine carbonate sediments are often taken as evidence for diagenetic alteration, as it is difficult to produce such arrays in a primary depositional environment (Marshall, 1992; Melim, Swart & Eberli, 2004; Knauth & Kennedy, 2009; Preto, Spotl & Guaiumi, 2009). At Tianfengping, there is a weak covariation between $\delta^{13}C_{carb}$ and $\delta^{18}O_{carb}$ values ($R^2 = 0.25$, Fig. 8a) in the Maokou Formation, recording a primary seawater signal. However, the negative shift of $\delta^{13}C_{carb}$ profile at the top of the Maokou Formation is associated with the similar negative shift of $\delta^{18}O_{carb}$ profile (Fig. 7), suggesting a diagenetic origin in this interval although the rest of the Maokou Formation shows uniform $\delta^{13}C_{carb}$ values at 3.5‰, which is close to the average $\delta^{13}C_{carb}$ value of the Capitanian deposits (*c.* 4‰, Buggisch *et al.* 2015) and records a primary signal. The diagenetic dolostone succession in the uppermost Maokou Formation is just below a regional unconformity at the Maokou–Kuhfeng formations boundary, which is characterized by a palaeokarst (Fig. 3e, f), probably also indicating a diagenetic origin of $\delta^{13}C_{carb}$ at the top of this formation (e.g. Joachimski, 1994). However, there is no correlation between $\delta^{13}C_{carb}$ and $\delta^{18}O_{carb}$ ($R^2 = 0.10$, Fig. 8a) in the Wuchiaping Formation, suggesting a primary signal. The primary $\delta^{13}C_{carb}$ values in the Wuchiaping Formation are much lower than in the Maokou Formation.

5.b.2. $\delta^{13}C_{org}$ changes

Organic carbon was drawn from the same dissolved inorganic carbon (DIC) of carbonate during photosynthesis. However, the negative correlation between $\delta^{13}C_{org}$ and $\delta^{13}C_{carb}$ ($R^2 = 0.62$, Fig. 8b) suggests that other factors such as organic sources can also control the $\delta^{13}C_{org}$ changes. The heavy $\delta^{13}C_{org}$ values in the dolostone succession in the uppermost Maokou Formation, coincident with the occurrence of bitumen (Fig. 7) and the similar values of $\delta^{13}C_{org}$ between the dolostone succession and the overlying Kuhfeng chert, suggest that the hydrocarbon bitumen was probably derived from the Kuhfeng Formation, a hydrocarbon source rock in South China (Liu *et al.* 2014), affected the $\delta^{13}C_{org}$ in the dolostone succession. The $\delta^{13}C_{org}$ values (*c.* 22‰) of sandstones and claystones in swamp facies in the lower Wangpo Shale Member are much heavier than the $\delta^{13}C_{org}$ of the Kuhfeng chert in the moderate-water-depth shelf facies. This suggests an input of terrestrial organic matter sources in the lower Wangpo Shale Member since marine organic carbon older than Oligocene age is isotopically lighter than the land-derived carbon (Galimov, 2006). Furthermore, the $\delta^{13}C_{org}$ values in the upper Wangpo Shale Member and the lower Xiayao Limestone Member deposited in a restricted environment near coastline are heavier than the $\delta^{13}C_{org}$ values in the upper Xiayao Limestones deposited in open marine. This also suggests a more terrestrial ^{13}C-rich organic matter input in the former. The input of terrestrial organic matter therefore controls the $\delta^{13}C_{org}$ changes at Tianfengping.

5.c. Carbon isotopic changes and their implication for mass extinction

The carbon-isotope correlation between the Tianfengping section and the Tieqiao section displays: (1) a similar trend of $\delta^{13}C_{org}$ between these two sections; (2) a positive peak at the Maokou–Heshan formation boundary or the Kuhfeng–Wuchiaping formation boundary; and (3) similar values of $\delta^{13}C_{carb}$ in the upper Maokou Formation and the lower Wuchiapingian between these two sections (Fig. 9). These similarities suggest the $\delta^{13}C_{carb}$ and $\delta^{13}C_{org}$ changes represent regional signals at least since these two sections are

https://doi.org/10.1017/S0016756817000462 Published online by Cambridge University Press

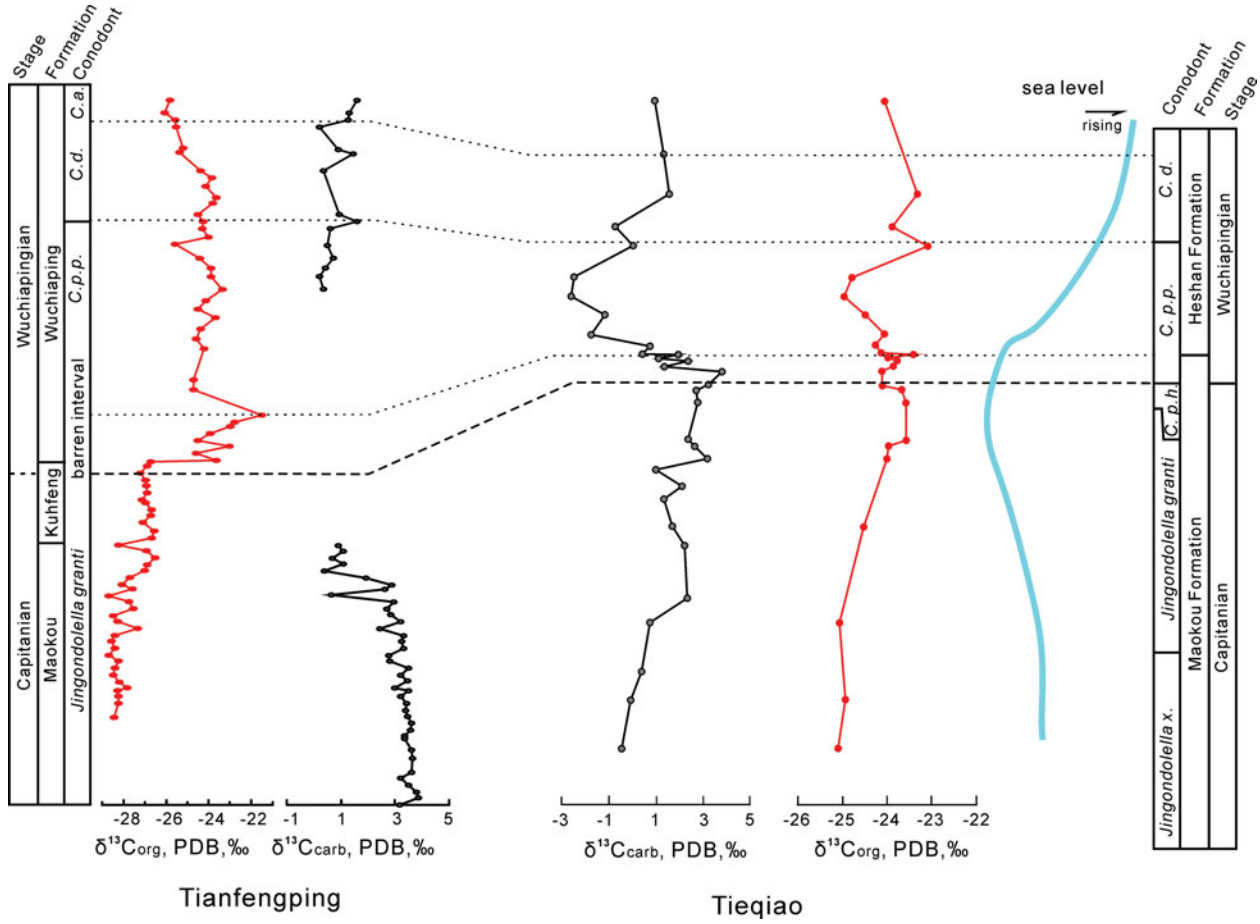

Figure 9. (Colour online) Carbon-isotope correlation between the Tianfengping section in Hubei Province of South China and the Tieqiao section in Laibin in Guangxi Province of South China. Organic- and inorganic-carbon isotope data at Tieqiao from Yan, Zhang & Qiu (2013). Sea-level change at Tieqiao is from Qiu *et al.* (2014) and Haq & Schutter (2008).

c. 730 km apart from each other. The clastic-origin tuff/claystones in the lowermost Heshan Formation at Tieqiao are related to Emeishan volcanism (Zhong, He & Xu, 2013). The tuff sandstone/claystones in the Wangpo Shale Member at Tianfengping (Fig. 9) is also related to the Emeishan volcanism (cf. Isozaki *et al.* 2008; He *et al.* 2010; Deconinck *et al.* 2014). The negative shift of $\delta^{13}C_{org}$ values at the G–L boundary at Tieqiao can be correlated to the same small negative shift (*c.* 0.5 ‰ in magnitude) of $\delta^{13}C_{org}$ values in the upper Kuhfeng Formation at Tianfengping. Combined with the conodont zones, the G–L boundary at Tianfengping is probably in the upper Kuhfeng Formation (Fig. 9). The gradual negative shift of $\delta^{13}C_{org}$ in the Xiayao Limestone Member in the upper Wuchiaping Formation at Tianfengping can be correlated to the similar negative shift of $\delta^{13}C_{org}$ in the *Clarkina dukouensis* conodont zone at Tieqiao (Fig. 9).

The $\delta^{13}C_{carb}$ in the lower Wuchiapingian represents a primary signal and is much lighter (*c.* 3.0 ‰ in magnitude) than that in the lower and middle Maokou Formation, which also records a primary signal. Previous studies have suggested that the lower $\delta^{13}C_{carb}$ values in the lower Wuchiapingian strata were controlled by: (1) volcanism and/or thermo-metamorphism methane (Wignall *et al.* 2009*a*; Wei *et al.* 2012); (2) low biologic productivity or declined photosynthesis (Isozaki, Kawahata & Ota, 2007; Yan, Zhang & Qiu, 2013; Nishikane *et al.* 2014); (3) shallow-marine anoxia (Saitoh *et al.* 2013*a* , 2014, 2017; Zhang *et al.* 2015; Wei *et al.* 2016); and (4) re-oxidation of ^{12}C-enriched organic material due to eustatic sea-level falling (Lai *et al.* 2008). Lithic arenites with abundant tuff grains in the Wangpo Shale Member in the lower Wuchiaping Formation at Tianfengping (Fig. 3) suggest a volcanic eruption related to the Emeishan large igneous province (LIP) (Fig. 5). Generally, large basalt volcanism releases abundant ^{12}C-enriched CO_2 into atmosphere (Hansen, 2006). However, according to the model calculation by Berner (2002), the Siberian LIP can only yield *c.* 1.0–1.7 ‰ magnitude negative excursion in one million years. The much smaller Emeishan LIP eruption may not yield this large gradual negative change in $\delta^{13}C_{carb}$ values in the lower Wuchiapingian because small volumes of greenhouse gases need to be released extremely quickly (Jost *et al.* 2014).

Declined primary productivity decreases the ^{12}C-enriched organic matter burial, resulting in a negative excursion of inorganic-carbon isotope (Magaritz, 1989; Broecker & Peacock, 1999; Twitchett *et al.* 2001; Korte & Kozur, 2010). This idea had been applied to explain the negative excursion of $\delta^{13}C_{carb}$

across the G–L boundary at Tieqiao by Yan, Zhang & Qiu (2013). However, the widespread black shale (Wangpo Shale Member) in the lower Wuchiaping Formation is enriched in organic matter in the South China (e.g. at Tianfengping) and North China blocks. In addition, there were widespread coal beds at the G–L boundary across the South China Block. The low value of $\delta^{13}C_{carb}$ in the lower Wuchiapingian at Tianfengping is therefore associated with high organic matter succession instead of low organic matter, suggesting that low primary productivity may not be the cause for this negative excursion.

The upwards rising of chemocline permits the return of isotopically light carbon to shallow-water depths, resulting in a fall of $\delta^{13}C_{carb}$ in shallow-water (Küspert, 1982, p. 482; Algeo *et al.* 2007). The shallow-marine anoxia had been suggested to be the cause of the negative excursion of $\delta^{13}C_{carb}$ across the G–L boundary Saitoh *et al.* (2013*a*). However, the strongest anoxia at the G–L boundary at Laibin (Wei *et al.* 2016) is not associated with the negative excursion of $\delta^{13}C_{carb}$ (Yan, Zhang & Qiu, 2013), suggesting that the anoxia may not have been a major cause for this carbon-isotope shift.

During global sea-level fall, ^{12}C-enriched organic matter may have been oxidized at exposed continental shelves and transported into the ocean (Holser & Magaritz, 1987, 1992; Baud, Magaritz & Holser, 1989). The heavier values of $\delta^{13}C_{org}$ occurring in the coastal environments instead of the open shallow-marine environments at Tianfengping indicates that the input of terrestrial organic matter controls the $\delta^{13}C_{org}$ changes (e.g. Siegert *et al.* 2011; Kraus *et al.* 2013) because marine organic carbon older than Oligocene age is isotopically lighter than the land-derived carbon (Galimov, 2006) and Permian wood shows heavier $\delta^{13}C$ values than coeval marine-sourced organic matter (Foster *et al.* 1997; Krull, 1999; Korte *et al.* 2001; Ward *et al.* 2005; Hermann *et al.* 2010). The negative correlation between $\delta^{13}C_{carb}$ and $\delta^{13}C_{org}$ ($R^2 = 0.62$, Fig. 8) therefore suggests that low $\delta^{13}C_{carb}$ values correspond to relatively high $\delta^{13}C_{org}$ values during/or immediately after regression which brings more terrestrial organic matter input and results in high values of $\delta^{13}C_{org}$ at Tianfengping or even in South China. Large-scale regression during the G–L transition enhanced the oxidization of exposed organic matter or soil, resulting in a high input of ^{12}C-rich DIC via river runoff. In South China, the unconformity at the G–L boundary is regional (He *et al.* 2003, 2006; Shen *et al.* 2007) and represents a regional to global sea-level fall (Shen *et al.* 2007; Wignall *et al.* 2012; Qiu *et al.* 2014). This large-scale global regression (Haq & Schutter, 2008) is associated with the widespread negative excursion of $\delta^{13}C_{carb}$ in South China (Wang, Cao & Wang, 2004; Lai *et al.* 2008; Bond *et al.* 2010), Japan (Isozaki, Kawahata & Minoshima, 2007; Isozaki, Kawahata & Ota, 2007) and Iran (Shen *et al.* 2013), probably suggesting an impact of regression on this carbon-isotope change. At Tianfengping, the Kuhfeng–Wuchiaping formation boundary and the Maokou–Kuhfeng formation boundary represent regional unconformities and reflect large-scale sea-level fall. These two pulses of regression may correspond to the two episodes of Emeishan eruption evidenced by two basalt successions separated by a siliceous limestone succession at Xiongjiachang in Guizhou Province, South China (e.g. Wignall *et al.* 2009*a*). Sea-level fall and re-oxidized organic matter may therefore be the main controlling factor of this negative shift of $\delta^{13}C_{carb}$ in lower Wuchiapingian strata. Qiu *et al.* (2013) reported two pulses of carbon isotope excursion during middle Capitanian time and at the G–L boundary in South China, corresponding to two pulses of regression. The mechanism of re-oxidized organic matter can also be used to explain the first pulse of $\delta^{13}C_{carb}$ negative excursion during middle Capitanian time. This sea-level fall coincides with the disappearance of foraminifers and fusulinids at Tianfengping (Fig. 6), suggesting that sea-level fall may be the cause of the biotic crisis at the G–L boundary via the loss of shallow-marine habitat where benthos lived (e.g. Qiu *et al.* 2014).

6. Conclusions

The negative shift of $\delta^{13}C_{carb}$ in the uppermost Maokou Formation at Tianfengping in South China is of diagenetic origin. However, the $\delta^{13}C_{carb}$ values in the main part of the Maokou Formation and in the Wuchiaping Formation represent primary signals of coeval sea water. Bulk organic-carbon isotope changes at Tianfengping mainly reflect the shift of organic matter sources, that is, the increased contribution of terrestrial organic matter. Sea-level fall led to high terrestrial organic matter input and resulted in heavy $\delta^{13}C_{org}$ values. The 3.0 ‰-magnitude lower $\delta^{13}C_{carb}$ in the Wuchiaping Formation compared to that in the lower–middle Maokou Formation at Tianfengping was probably caused by the re-oxidized ^{12}C-rich organic matter or soil during sea-level fall. Large-scale global regression resulted in the decrease of $\delta^{13}C_{carb}$ in lower Wuchiapingian strata and led to the disappearance of foraminifers and fusulinids during Capitanian time in South China.

Acknowledgements. We thank two anonymous reviewers and the editor Paul Upchurch for their constructive comments and suggestions. This work was financially supported by the National Natural Science Foundation of China (grant no. 41302021). We thank Zhijun Zhu's suggestions for mineral identification.

References

Algeo, T. J., Ellwood, B., Nguyen, T. K. T., Rowe, H. & Maynard, J. B. 2007. The Permian-Triassic boundary at Nhi Tao, Vietnam: Evidence for recurrent influx of sulfidic watermasses to a shallow-marine carbonate platform. *Palaeogeography, Palaeoclimatology, Palaeoecology* **252**, 304–27.

Ali, J. R., Thompson, G. M., Zhou, M. F. & Song, X. 2005. Emeishan large igneous province, SW China. *Lithos* **79**, 475–89.

Baud, A., Magaritz, M. & Holser, W. T. 1989. Permian-Triassic of the Tethys: Carbon isotope studies. *Geologische Rundschau* **78**, 649–77.

Berner, R. A. 2002. Examination of hypotheses for the Permo-Triassic boundary extinction by carbon cycle modeling. *Proceedings of the National Academy of Sciences of the United States of America* **99**, 4172–7.

Bond, D. P. G., Wignall, P. B., Joachimski, M. M., Sun, Y., Savov, I., Grasby, S. E., Beauchamp, B. & Blomeier, D. P. G. 2015. An abrupt extinction in the middle Permian (Capitanian) of the Boreal Realm (Spitsbergen) and its link to anoxia and acidification. *GSA Bulletin* **127**, 1411–21.

Bond, D. P. G., Wignall, P. B., Wang, W., Izon, G., Jiang, H., Lai, X., Sun, Y., Newton, R. J., Shao, L., Védrine, S. & Cope, H. 2010. The mid-Capitanian (Middle Permian) mass extinction and carbon isotope record of South China. *Palaeogeography, Palaeoclimatology, Palaeoecology* **292**, 282–94.

Broecker, W. S. & Peacock, S. 1999. An ecologic explanation for the Permo-Triassic carbon and sulfur isotope shifts. *Global Biogeochemical Cycles* **13**, 1167–72.

Buggisch, W., Krainer, K., Schaffhauser, M., Joachimski, M. & Korte, C. 2015. Late Carboniferous to Late Permian carbon isotope stratigraphy: A new record from post-Variscan carbonates from the Southern Alps (Austria and Italy). *Palaeogeography, Palaeoclimatology, Palaeoecology* **433**, 174–90.

Chen, B., Joachimski, M. M., Sun, Y., Shen, S. & Lai, X. 2011. Carbon and conodont apatite oxygen isotope records of Guadalupian-Lopingian boundary sections: Climatic or sea-level signal? *Palaeogeography, Palaeoclimtology, Palaeoecology* **311**, 145–53.

Chen, L., Li, Z., Huang, Z., Zhang, K. & Duan, W. 2000. Discovery of the clastic rocks in the basal part of the Permian Gufeng Formation in Huangyan, Jianshi, Hubei and its significance. *Journal of Stratigraphy* **24**, 207–9 (in Chinese with English abstract).

Chen, W., Liu, J., Wang, Z. & Zheng, Q. 2003. Study on lithofacies palaeogeography during the Permian Emeishan basalt explosion in Guizhou Province. *Journal of Palaeogeography* **5**, 17–28 (in Chinese with English abstract).

Chen, Z. Q., George, A. D. & Yang, W. R. 2009. Effects of Middle-Late Permian sea-level changes and mass extinction on the formation of the Tieqiao skeletal mound in the Laibin area, South China. *Australian Journal of Earth Sciences* **56**, 745–63.

Clapham, M. E., Shen, S. & Bottjer, D. J. 2009. The double mass extinction revisited: reassessing the severity, selectivity, and causes of the end-Guadalupian biotic crisis (Late Permian). *Paleobiology* **35**, 32–50.

Courtillot, V. 1999. *Evolutionary Catastrophes: The Science of Mass Extinction*. Cambridge: Cambridge University Press, 237 pp.

Deconinck, J. F., Craquin, S., Bruneau, L., Pellenard, P., Baudin, F. & Feng, Q. 2014. Diagenesis of claystone minerals and K-bentonites in Late Permian/Early Triassic sediments of the Sichuan Basin (Chaotian section, Central China). *Journal of Asian Earth Sciences* **81**, 28–37.

Du, X., Song, X., Zhang, M., Lu, Y., Lu, Y., Chen, P., Liu, Z. & Yang, S. 2015. Shale gas potential of the Lower Permian Gufeng Formation in the western area of the Lower Yangtze Platform, China. *Marine and Petroleum Geology* **67**, 526–43.

Feng, Z., Yang, Y. & Jin, Z. 1997. *Lithofacies Paleogeography of Permian of South China*. Dongying: Petroleum University Press, 75 pp. (in Chinese).

Foster, C. B., Logan, G. A., Summons, R. E., Gorter, J. D. & Edwards, D. S. 1997. Carbon isotopes, kerogen types and the Permian-Triassic boundary in Australia: Implications for exploration. *Australian Petroleum Production and Exploration Association Journal* **37**, 472–89.

Galimov, E. M. 2006. Isotope organic geochemistry. *Organic Geochemistry* **37**, 1200–62.

Hada, S., Khosithanont, S., Goto, H., Fontaine, H. & Salyapongse, S. 2015. Evolution and extinction of Permian fusulinid fauna in the Khao Tham Yai Limestone in NE Thailand. *Journal of Asian Earth Sciences* **104**, 175–84.

Hansen, H. J. 2006. Stable isotopes of carbon from basaltic rocks and their possible relation to atmospheric isotope excursions. *Lithos* **92**, 105–16.

Haq, B. U. & Schutter, S. R. 2008. A chronology of Paleozoic sea-level changes. *Science* **322**, 64–8.

He, B., Xu, Y., Chung, S., Xiao, L. & Wang, Y. 2003. Sedimentary evidence for a rapid, kilometer-scale crustal doming prior to the eruption of the Emeishan flood basalts. *Earth and Planetary Science Letters* **213**, 391–405.

He, B., Xu, Y., Wang, Y. & Luo, Z. 2006. Sedimentary and lithofacies paleogeography in Southwestern China before and after the Emeishan flood volcanism: New insights into surface response to mantle plume activity. *Journal of Geology* **114**, 117–32.

He, B., Xu, Y. G., Zhong, Y. T. & Guan, J. P. 2010. The Guadalupian-Lopingian boundary mudstones at Chaotian (SW China) are clastic rocks rather than acidic tuffs: implication for a temporal coincidence between the end-Guadalupian mass extinction and the Emeishan volcanism. *Lithos* **119**, 10–19.

Hermann, E., Hochuli, P. A., Bucher, H., Vigran, J. O., Weissert, H. & Bernasconi, S. M. 2010. A close-up view of the Permian-Triassic boundary based on expanded organic carbon isotope records from Norway (Trøndelag and Finnmark Platform). *Global and Planetary Change* **74**, 156–67.

Holser, W. T. & Magaritz, M. 1987. Events near the Permian-Triassic boundary. *Modern Geology* **11**, 155–80.

Holser, W.T. & Magaritz, M. 1992. Cretaceous/Tertiary and Permian/Triassic boundary events compared. *Geochimica et Cosmochimica Acta* **56**, 3297–309.

Isozaki, Y. 1997. Permo-Triassic boundary superanoxia and stratified superocean: Record from lost deep sea. *Science* **276**, 235–8.

Isozaki, Y. & Aljinović, D. 2009. End-Guadalupian extinction of the Permian gigantic bivalve Alatoconchidae: end of gigantism in tropical seas by cooling. *Palaeogeography, Palaeoclimatology, Palaeoecology* **284**, 11–21.

Isozaki, Y., Aljinovic, D. & Kawahata, H. 2011. The Guadalupian (Permian) Kamura event in European Tethys. *Palaeogeography, Palaeoclimatology, Palaeoecology* **308**, 12–21.

Isozaki, Y., Kawahata, H. & Minoshima, K. 2007. The Capitanian (Permian) Kamura cooling event: the beginning of the Paleozoic-Mesozoic transition. *Palaeoworld* **16**, 16–30.

Isozaki, Y., Kawahata, H. & Ota, A. 2007. A unique carbon isotope record across the Guadalupian-Lopingian

(Middle-Upper Permian) boundary in mid-oceanic paleo-atoll carbonates: the high-productivity "Kamura event" and its collapse in Panthalassa. *Global and Planetary Science Change* **55**, 21–38.

ISOZAKI, Y., YAO, J., JI, Z., SAITOH, M., KOBAYASHI, N. & SAKAI, H. 2008. Rapid sea-level change in the Late Guadalupian (Permian) on the Tethyan side of Sout China: litho- and biostratigraphy of the Chaotian section in Sichuan. *Proceedings of the Japan Academy Series B* **84**, 344–53.

JIN, Y., SHEN, S., HENDERSON, C. M., WANG, X., WANG, W., WANG, Y., CAO, C. & SHANG, Q. 2006. The Global Stratotype Section and Point (GSSP) for the boundary between the Capitanian and Wuchiapingian Stage (Permian). *Episodes* **29**, 253–62.

JIN, Y., ZHANG, J. & SHANG, Q. 1994. Two phases of the end-Permian mass extinction. *Canadian Society of Petroleum Geologists* **17**, 813–22.

JOACHIMSKI, M. M. 1994. Subaerial exposure and deposition of shallowing upward sequences: evidence from stable isotopes of Purbeckian pertidal carbonates (basal Cretaceous), Swiss and French Jura Mountains. *Sedimentology* **41**, 805–24.

JOST, A. B., MUNDIL, R., HE, B., BROWN, S. T., ALTINER, D., SUN, Y., DEPAOLO, D. J. & PAYNE, J. L. 2014. Constraining the cause of the end-Guadalupian extinction with coupled records of carbon and calcium isotopes. *Earth and Planetary Science Letters* **396**, 201–12.

KAMETAKA, M., TAKEBE, M., NAGAI, H., ZHU, S. & TAKAYANAGI, Y. 2005. Sedimentary environments of the Middle Permian phosphorite-chert complex from the northeastern Yangtze platform, China; the Gufeng Formation: a continental shelf radiolarian chert. *Sedimentary Geology* **174**, 197–222.

KNAUTH, L. P. & KENNEDY, M. J. 2009. The late Precambrian greening of the Earth. *Nature* **460**, 728–32.

KOBAYASHI, F. 2012. Middle and Late Permian foraminifers from the Chichibu belt, Takachiho area, Kyushu, Japan: Implications for faunal events. *Journal of Paleontology* **86**, 669–87.

KOFUKUDA, D., ISOZAKI, Y. & IGO, H. 2014. A remarkable sea-level drop and relevant biotic responses across the Guadalupian-Lopingian (Permian) boundary in low-latitude mid-Panthalassa: Irreversible changes recorded in accreted paleo-atoll limestones in Akasaka and Ishiyama, Japan. *Journal of Asian Earth Sciences* **82**, 47–65.

KORTE, C. & KOZUR, H. 2010. Carbon-isotope stratigraphy across the Permian-Triassic boundary: a review. *Journal of Asian Earth Sciences* **39**, 215–35.

KORTE, C., VEIZER, J., LEYTHAEUSER, D., BELOW, R. & SCHWARK, L. 2001. Evolution of Permian and Lower Triassic $\delta^{13}C$ in marine and terrigenous organic material. *Terra Nostra* **4**, 30–4.

KOZUR, H. 1993. Upper Permian radiolaria from the Sosio Valley area, western Sicily (Italy) and from the uppermost Lamar Limestone of West Texas. *Jahrbuch der Geologischen Bundesanstalt Wien* **136**(1), 99–123.

KRAUS, S. H., BRANDNER, R., HEUBECK, C., KOZUR, H. W., STRUCK, U. & KORTE, C. 2013. Carbon isotope signatures of latest Permian marine successions of the Southern Alps suggest a continental runoff pulse enriched in land plant material. *Fossil Record* **16**(1), 97–109.

KRULL, E. S. 1999. Permian palsa mires as palaeoenvironmental proxies. *Palaios* **14**, 530–44.

KÜSPERT, W. 1982. Environmental changes during oil shale deposition as deduced from stable isotope ratios. In *Cyclic and Event Stratification* (eds G. Einsele & A. Seilacher), pp. 482–501. Berlin: Springer.

LAI, X., WANG, W., WIGNALL, P. B., BOND, D. P. G., JIANG, H., ALI, J. R., JOHN, E. H. & SUN, Y. 2008. Palaeoenvironmental change during the end-Guadalupian (Permian) mass extinction in Sichuan, China. *Palaeogeography, Palaeoclimatology, Palaeoecology* **269**, 78–93.

LIU, G., JIN, Z., LUO, K. & PENG, J. 2014. Oil and source correlation in Huangqiao and Jurong areas, Lower Yangtze region. *Petroleum Geology & Experiment* **36**(3), 359–66 (in Chinese with English abstract).

MAGARITZ, M. 1989. ^{13}C minima follow extinction events: a clued to faunal radiation. *Geology* **17**, 337–40.

MARSHALL, J. D. 1992. Climatic and oceanographic isotopic signals from the carbonate rock record and their preservation. *Geological Magazine* **129**, 143–60.

MELIM, L. A., SWART, P. K. & EBERLI, G. P. 2004. Mixing-zone diagenesis in the subsurface of Florida and the Bahamas. *Journal of Sedimentary Research* **74**, 904–13.

MUTTONI, G., GAETANI, M., KENT, D., SCIUNNACH, D., ANGIOLINI, L., BERRA, F., GARZANTI, E., MATTEI, M. & ZANCHI, A. 2009. Opening of the NeoTethys Ocean and the Pangea B to Pangea A transformation during the Permian. *GeoArabia* **14**(4), 17–48.

NISHIKANE, Y., KAIHO, K., HENDERSON, C. M., TAKAHASHI, S. & SUZUKI, N. 2014. Guadalupian-Lopingian conodont and carbon isotope stratigraphies of a deep chert sequence in Japan. *Palaeogeography, Palaeoclimatology, Palaeoecology* **403**, 16–29.

NIU, Z., DUAN, Q., FU, T., XU, A., ZENG, B. & ZHU, Y. 2000. Paleokarst unconformity on top of the Maokou Formation in the Jianshi-Badong area, Hubei: its discovery and significance. *Regional Geology of China* **19**, 276–81 (in Chinese with English abstract).

PRETO, N., SPOTL, C. & GUAIUMI, C. 2009. Evaluation of bulk carbonate delta C-13 data from Triassic hemipelagites and the initial composition of carbonate mud. *Sedimentology* **56**, 1329–45.

QIU, Z., WANG, Q., ZOU, C., YAN, D. & HOU, L. 2013. Carbon isotope negative excursion and its significance during the Middle–Late Permian transition in the Laibin area. *Geological Review* **59**(supp.), 1228–31 (in Chinese).

QIU, Z., WANG, Q., ZOU, C., YAN, D. & WEI, H. 2014. Transgressive-regressive sequences on the slope of an isolated carbonate platform (Middle-Late Permian, Laibin, South China). *Facies* **60**, 327–45.

ROSALES, I., QUESADA, S. & ROBLES, S. 2001. Primary and diagenetic isotopic signals in fossils and hemipelagic carbonates: the lower Jurassic of northern Spain. *Sedimentology* **48**, 1149–69.

SAITOH, M., ISOZAKI, Y., UENO, Y., YOSHIDA, N., YAO, J. & JI, Z. 2013a. Middle-Upper Permian carbon isotope stratigraphy at Chaotian, South China: Pre-extinction multiple upwelling of oxygen-depleted water onto continental shelf. *Journal of Asian Earth Sciences* **67–8**, 51–62.

SAITOH, M., ISOZAKI, Y., YAO, J., JI, Z., UENO, Y. & YOSHIDA, N. 2013b. The appearance of an oxygen-deplete condition on the Capitanian disphotic slope/basin in South China: Middle-Upper Permian stratigraphy at Chaotian. *Global and Planetary Change* **105**, 180–92.

SAITOH, M., UENO, Y., ISOZAKI, Y., NISHIZAWA, M., SHOZUGAWA, K., KAWAMURA, T., YAO, J., JI, Z., TAKAI, K., YOSHIDA, N. & MATSUO, M. 2014. Isotopic evidence for water-column denitrification and sulfate reduction at the end-Guadalupian (Middle Permian). *Global and Planetary Change* **123**, 110–20.

Saitoh, M., Ueno, Y., Matsu'ura, F., Kawamura, T., Isozaki, Y., Yao, J., Ji, Z. & Yoshida, N. 2017. Multiple sulfur isotope records at the end-Guadalupian (Permian) at Chaotian, China: implications for a role of bioturbation in the Phanerozoic sulfur cycle. *Journal of Asian Earth Sciences* **135**, 70–9.

Scotese, C. R. & Langford, R. P. 1995. Pangea and paleogeography of the Permian. In *The Permian of Northern Pangea* (eds P. A. Scholle, T. M. Peryt & D. S. Ulmer-Scholle), pp. 3–19. Berlin: Springer, vol. 1.

Shen, S. Z., Cao, C., Zhang, H., Bowring, S. A., Henderson, C. M., Payne, J. L., Davydov, V. I., Chen, B., Yuan, D., Zhang, Y., Wang, W. & Zheng, Q. 2013. High-resolution δ;$^{13}C_{carb}$ chemostratigraphy from latest Guadalupian through earliest Triassic in South China and Iran. *Earth and Planetary Science Letters* **375**, 156–65.

Shen, S. Z. & Shi, G. R. 1996. Diversity and extinction patterns of Permian brachiopoda of South China. *Historical Biology* **12**, 93–110.

Shen, S. Z. & Shi, G. R. 2002. Paleobiogeographical extinction patterns of Permian brachiopods in the Asian-western Pacific Region. *Paleobiology* **28**, 449–63.

Shen, S. Z., Wang, Y., Henderson, C. M., Cao, C. & Wang, W. 2007. Biostratigraphy and lithofacies of the Permian System in the Laibin-Heshan area of Guangxi, South China. *Palaeoworld* **16**, 120–39.

Shi, L., Feng, Q., Shen, J., Ito, T. & Chen, Z. Q. 2016. Proliferation of shallow-water radiolarian coinciding with enhanced oceanic productivity in reducing conditions during the Middle Permian, South China: evidence from the Gufeng Formation of western Hubei Province. *Palaeogeography, Palaeoclimatology, Palaeoecology* **444**, 1–14.

Siegert, S., Kraus, S.H., Mette, W., Struck, U. & Korte, C. 2011. Organic carbon isotope values from the Late Permian Seis/Siusi succession (Dolomites, Italy): Implications for palaeoenvironmental changes. *Fossil Record* **14**, 207–17.

Stanley, S. M. & Yang, X. 1994. A double mass extinction at the end of the Paleozoic Era. *Science* **266**, 1340–4.

Sun, Y., Lai, X., Wignall, P. B., Widdowson, M., Ali, J., Jiang, H., Wang, W., Yan, C., Bond, D. P. G. & Védrine, S. 2010. Dating the onset and nature of the Middle Permian Emeishan large igneous province eruptions in SW China using conodont biostratigraphy and its bearing on mantle plume uplift models. *Lithos* **119**, 20–33.

Twitchett, R. J., Looy, C. V., Morante, R., Visscher, H. & Wignall, P. B. 2001. Rapid and synchronous collapse of marine and terrestrial ecosystems during the end-Permian biotic crisis. *Geology* **29**, 351–4.

Wang, W., Cao, C. & Wang, Y. 2004. The carbon isotope excursion on GSSP candidate section of Lopingian-Guadalupian boundary. *Earth and Planetary Science Letters* **220**, 57–67.

Wang, X. & Sugiyama, T. 2000. Diversity and extinction patterns of the Permian corals in China. *Lethaia* **33**, 285–94.

Wang, Y. & Jin, Y. 2000. Permian palaeogeographic evolution of the Jiangnan Basin, South China. *Palaeogeography, Palaeoclimatology, Palaeoecology* **160**, 35–44.

Ward, P. D., Botha, J., Buick, R., De Kock, M. O., Erwin, D. H., Garison, G. H., Kirschvink, J. L. & Smith, R. 2005. Abrupt and gradual extinction among Late Permian land vertebrates in the Karoo Basin, South Africa. *Science* **307**, 709–14.

Wei, H., Chen, D., Yu, H. & Wang, J. 2012. End-Guadalupian mass extinction and negative carbon isotope excursion at Xiaojiaba, Guangyuan, Sichuan. *Science China Earth Science* **55**, 1480–8.

Wei, H., Wei, X., Qiu, Z., Song, H. & Shi, G. 2016. Redox conditions across the G-L boundary in South China: evidence from pyrite morphology and sulfur isotopic compositions. *Chemical Geology* **440**, 1–14.

Weidlich, O. 2002. Permian reefs re-examined: extrinsic control mechanisms of gradual and abrupt changes during 40 my of reef evolution. *Geobios Mémoire Spécial* **24**, 287–94.

Weissert, H., Joachimski, M. & Sarnthein, M. 2008. Chemostratigraphy. *Newsletters on Stratigraphy* **42**, 145–79.

Wignall, P. B., Bond, D. P. G., Haas, J., Wang, W., Jiang, H., Lai, X., Altiner, D., Védrine, S., Hips, K., Zajzon, N., Sun, Y. & Newton, R. J. 2012. Capitanian (middle Permian) mass extinction and recovery in western Tethys: a fossil, facies, and $\delta^{13}C$ study from Hungary and Hydra Island (Greece). *Palaios* **27**, 78–89.

Wignall, P. B., Sun, Y., Bond, D. P. G., Izon, G., Newton, R. J., Védrine, S., Widdowson, M., Ali, J. R., Lai, X., Jiang, H., Cope, H. & Bottrell, S. H. 2009a. Volcanism, mass extinction, and carbon isotope fluctuations in the Middle Permian of China. *Science* **324**, 1179–82.

Wignall, P. B., Védrine, S., Bond, D. P. G., Wang, W., Lai, X., Ali, J. R. & Jiang, H. 2009b. Facies analysis and sea-level change at the Guadalupian-Lopingian Global Stratotype (Laibin, South China), and its bearing on the end-Guadalupian mass extinction. *Journal of the Geological Society, London* **166**, 655–66.

Xia, W., Zhang, N., Kakuwa, Y. & Zhang, L. 2006. Radiolarian and conodont biozonation in the pelagic Guadalupian-Lopingian boundary interval at Dachongling,Guangxi, South China, and mid-upper Permian global correlation. *Stratigraphy* **2**, 217–38.

Xu, Y., Chung, S., Jahn, B. M. & Wu, G. 2001. Petrologic and geochemical constraints on the petrogenesis of Permian-Triassic Emeishan flood basalts in southwestern China. *Lithos* **58**, 145–68.

Yan, D., Zhang, L. & Qiu, Z. 2013. Carbon and sulfur isotopic fluctuations associated with the end-Guadalupian mass extinction in South China. *Gondwana Research* **24**, 1276–82.

Yao, L., Gao, Z., Yang, Z. & Long, H. 2002. Origin of seleniferous cherts in Yutangba Se deposit, southwest Enshi, Hubei Province. *Science China Earth Science* **45**, 741–54.

Yin, H. F., Huang, S., Zhang, K., Hansen, H., Yang, F., Ding, M. & Bie, X. 1992. The effects of volcanism on the Permo-Triassic mass extinction in South China. In *Permo-Triassic Events in the Eastern Tethys* (ed. W. C. Sweet), pp. 146–57. Cambridge: Cambridge University Press.

Yin, H. F., Jiang, H., Xia, W., Feng, Q., Zhang, N. & Shen, J. 2014. The end-Permian regression in South China and its implication on mass extinction. *Earth-Science Reviews* **137**, 19–33.

Zhang, G., Zhang, X., Li, D., Farquhar, J., Shen, S., Chen, X. & Shen, Y. 2015. Widespread shoaling of sulfidic waters linked to the end-Guadalupian (Permian) mass extinction. *Geology* **43**, 1091–4.

Zhang, Z., Wang, Y. & Zheng, Q. 2015. Middle Permian smaller foraminifers from the Maokou Formation at the

Tieqiao section, Guangxi, South China. *Palaeoworld* **24**, 263–76.

ZHONG, Y. T., HE, B., MUNDIL, R. & XU, Y. G. 2014. CA-TIMS zircon U-Pb dating of felsic ignimbrite from the Binchuan section: Implications for the termination age of Emeishan large igneous province. *Lithos* **204**, 14–9.

ZHONG, Y. T., HE, B. & XU, Y. G. 2013. Mineralogy and geochemistry of claystones from the Guadalupian-Lopingian boundary at Penglaitan, South China: Insights into the pre-Lopingian geological events. *Journal of Asian Earth Sciences* **62**, 438–62.

ZHOU, M. F., MALPAS, J., SONG, X. Y., ROBINSON, P. T., SUN, M., KENNEDY, A. K., LESHER, C. M. & KEAYS, R. R. 2002. A temporal link between the Emeishan large igneous province (SW China) and the end-Guadalupian mass extinction. *Earth and Planetary Science Letters* **196**, 113–22.

ZHU, T. 1989. Sedimentological features and the genesis of lower Permian nodular and thin-bedded siliceous rocks in southern Anhui. *Journal of Palaeogeography* **43**(5), 1–8 (in Chinese with English abstract).